Surrogate-based Diffeomorphic Motion Estimation for Radiation Therapy: Comparison of Multivariate Regression Approaches

Matthias Wilms[a], René Werner[b], Jan Ehrhardt[a], Alexander Schmidt-Richberg[a], Maximilian Blendowski[a], and Heinz Handels[a]

[a]Institute of Medical Informatics, University of Lübeck, Lübeck, Germany
[b]Department of Computational Neuroscience, University Medical Center Hamburg-Eppendorf, Hamburg, Germany

ABSTRACT

Respiratory motion is a major source of error in radiation treatment of thoracic and abdominal tumors. State-of-the-art motion-adaptive radiation therapy techniques are usually guided by external breathing signals acting as surrogates for the internal motion of organs and tumors. Assuming a relationship between the surrogate measurements and the internal motion patterns, which are usually described by non-linear transformations, correspondence models can be defined and used for surrogate-based motion estimation. In this contribution, a diffeomorphic motion estimation framework based on standard multivariate linear regression is extended by subspace-based approaches like principal component analysis, partial least squares, and canonical correlation analysis. These methods aim at exploiting the hidden structure of the training data to improve the use of the information provided by high-dimensional surrogate and internal motion representations. A quantitative evaluation carried out on 4D CT data sets of 10 lung tumor patients shows that subspace-based approaches are able to significantly improve the mean estimation accuracy when compared to standard multivariate linear regression.

Keywords: correspondence modeling, motion estimation, regression, registration, radiotherapy

1. INTRODUCTION

Breathing-induced location uncertainties of target structures and associated organs at risk (OARs) are a major problem in radiation therapy (RT) of thoracic and abdominal tumors. Therefore, patient-specific information about breathing motion should be used during treatment planning and delivery to increase the precision of dose delivery. While 4D(=3D+t) CT data sets acquired for RT planning purposes provide insights into the breathing dynamics of the individual patient, they can not be used to steer motion-adaptive treatment approaches (respiratory gating or tumor tracking) in real-time. These advanced techniques are usually guided by an external breathing signal of a so-called surrogate (abdominal belt, spirometry, etc.), which can be easily acquired.[1,2]

Assuming a relationship between the time-dependent surrogate signal and the respiratory motion of internal structures, mathematical correspondence models can be defined, trained, and eventually be used to estimate the position of tumors and OARs given a surrogate measurement.[3] Due to the complex (three-dimensional) nature of internal motion and additional effects like, e.g., phase shifts and inter-cycle variations, the usage of simple one-dimensional signals (abdominal belt, spirometry, etc.) seems to be inadequate and motivates the introduction of multi-dimensional surrogates. Modern range imaging devices like Time-of-Flight (ToF) and structured light cameras provide an easy and contact-less way to monitor the lifting/raising of the chest wall in real-time without the use of artifical markers.[4] The acquired range images of the patient's skin surface can be seen as a multi-dimensional respiratory signal. In order to take advantage of such a high-dimensional surrogate signal and given the complex internal motion patterns, usually represented by non-linear transformations, adequate multivariate correspondence models have to be defined and evaluated.

Further author information: (Send correspondence to Matthias Wilms; E-mail: wilms@imi.uni-luebeck.de)

Medical Imaging 2013: Image Processing, edited by Sebastien Ourselin, David R. Haynor,
Proc. of SPIE Vol. 8669, 866915 · © 2013 SPIE · CCC code: 1605-7422/13/$18
doi: 10.1117/12.2002428

We have recently presented a diffeomorphic framework for surrogate-based motion estimation based on multivariate (multiple) linear regression (MLR).[5] Given a 4D CT image sequence, a patient-specific relation between corresponding surrogate measurements and internal motion patterns represented by previously estimated diffeomorphic non-linear transformations[6] can be trained. The advantage of restricting the transformations to diffeomorphisms is that they ensure the topology of the objects to be preserved, making them a natural choice for the intended application.[7] Furthermore, statistics on diffeomorphisms can be efficiently calculated within the Log-Euclidean framework proposed by Arsigny et al.[8]

Although the proposed MLR-based estimation approach can, in principle, be used with surrogate and internal motion signals of any dimensions, computational problems (multi-collinearities, etc.) frequently arise in practice due to the large amount of partially redundant data to be processed for high-dimensional surrogate and motion representations. With this in mind, this work focuses on the use of different subspace methods [principal components analysis (PCA), partial least squares (PLS), and canonical correlation analysis (CCA)] to tackle these problems. PCA has been utilized by several authors to develop correspondence models. For example, King et al.[9] and Zhang et al.[10] applied PCA to the motion data to obtain a low-dimensional parameterization of the complex lung motion. Furthermore, PCA has been applied to the surrogate data by Klinder et al.[11] in order to reduce multi-collinearities. Another option could be to combine both approaches by performing a PCA-based dimensionality reduction on both the motion and surrogate data separately before relating the PCA weights by an ordinary linear model. While this would result in compact correspondence models, a separate treatment of motion and surrogate data does not take their relationship into account. Therefore, some authors recommend the use of more elaborated methods like PLS[12] and CCA[13,14] to optimize the estimation accuracy. What has been missing so far is a comparison of all these subspace approaches. For that reason, this work aims to present them in a consistent way and to provide an extensive evaluation of the performance of these methods within our novel diffeomorphic motion estimation framework. Furthermore, we also investigate the influence of the dimensionality of the surrogate signal on the estimation accuracy.

2. METHODS

2.1 Diffeomorphic Framework for Surrogate-based Motion Estimation

In the following, let $(I_j)_{j\in\{1,\dots,n_{ph}\}}$ denote a 4D CT data set consisting of n_{ph} 3D images $I_j : \Omega \to \mathbb{R}$ ($\Omega \subset \mathbb{R}^3$), representing the patient's anatomy at states j of a breathing cycle. Furthermore, we assume a set of corresponding, synchronously acquired or retrospectively simulated n_{sur}-dimensional surrogate measurements $(\zeta_j)_{j\in\{1,\dots,n_{ph}\}}$, with $\zeta_j \in \mathbb{R}^{n_{sur}}$, to be given. Being interested in a diffeomorphic regression framework, the complex motion of internal structures between a reference breathing state I_1 and I_j is described by the non-linear transformation $\varphi_j = id + u_j : \Omega \to \Omega$ parameterized by a stationary velocity field v_j by $\varphi_j = \exp(v_j)$. It is estimated using a diffeomorphic registration scheme, which has been proven to be accurate for registration of lung CT images.[6]

From now on, we interpret the corresponding velocity fields v_j and surrogate measurements ζ_j as random variables $\mathbf{V}_j \in \mathbb{R}^{3m}$ (m is the number of image voxels) and $\mathbf{Z}_j \equiv \zeta_j$, respectively. Furthermore, let $\mathbf{V} := (\mathbf{V}_1^c, \dots, \mathbf{V}_{n_ph}^c)$ and $\mathbf{Z} := (\mathbf{Z}_1^c, \dots, \mathbf{Z}_{n_{ph}}^c)$ denote matrices consisting of the mean centered random variables $\mathbf{V}_j^c = \mathbf{V}_j - \overline{\mathbf{V}}$ and $\mathbf{Z}_j^c = \mathbf{Z}_j - \overline{\mathbf{Z}}$, which serve as training data for the estimation of the (supposed) linear relationship

$$\hat{\mathbf{V}} = \overline{\mathbf{V}} + \mathbf{B}(\hat{\mathbf{Z}} - \overline{\mathbf{Z}}) \tag{1}$$

between a surrogate signal observation $\hat{\mathbf{Z}} \equiv \hat{\zeta}$ (regressors) and the corresponding velocity field $\hat{\mathbf{V}}$ (regressands). Performing multivariate linear regression, an ordinary least squares (OLS) estimation of the regression coefficient matrix $\mathbf{B}$ is given by

$$\mathbf{B}^{OLS} = \arg\min_{\mathbf{B}'} \operatorname{tr}\Big[(\mathbf{V} - \mathbf{B}'\mathbf{Z})(\mathbf{V} - \mathbf{B}'\mathbf{Z})^T\Big] = \mathbf{V}\mathbf{Z}^T(\mathbf{Z}\mathbf{Z}^T)^{-1} = \mathbf{\Sigma_{VZ}}\mathbf{\Sigma_{ZZ}}^{-1}, \tag{2}$$

with $\mathbf{\Sigma_{ZZ}}$ being the covariance matrix of the surrogate signal observations $\mathbf{Z}$ and $\mathbf{\Sigma_{VZ}}$ denoting the cross-covariance matrix of $\mathbf{V}$ and $\mathbf{Z}$.[5,15] However, when dealing with high-dimensional surrogate signals, $\mathbf{\Sigma_{ZZ}}$ will usually be (nearly) rank deficient due to the linear relations of the different signal dimensions (multi-collinearities).

A common way to circumvent the possible non-invertibility is to approximate $\mathbf{\Sigma_{ZZ}}$ by $\mathbf{\Sigma_{ZZ}} + \gamma\mathbf{I}$, known as Tikhonov regularization. While this approach works well, the choice of the regularization parameter $\gamma > 0$ is rather heuristic and, in case of high-dimensional surrogate signals, inverting a large size matrix $\mathbf{\Sigma_{ZZ}} + \gamma\mathbf{I}$ remains computationally prohibitive. This motivates the usage of dimensionality reduction approaches, which can for example be used to project the data to a subspace, where the regressor covariance matrix can be easily inverted.

2.1.1 Regression based on Principal Component Analysis (PCA)

A classical approach for redundancy elimination is the principal component analysis (PCA).[16] First, a singular value decomposition (SVD) $\mathbf{Z} = \mathbf{UDW}^T$ is performed, where $\mathbf{U}$ and $\mathbf{V}$ are unitary matrices of left- and right-singular vectors of $\mathbf{Z}$, respectively, and $\mathbf{D}$ denotes a diagonal matrix with the corresponding singular values as its diagonal elements. Then, retaining only the first n_c left-singular vectors with positive singular values leads to a basis $\mathbf{U}_{n_c}$ of maximum data variation. Based on the approximation $\mathbf{\Sigma_{ZZ}} \approx \mathbf{U}_{n_c}(\mathbf{D}_{n_c}^T\mathbf{D}_{n_c})\mathbf{U}_{n_c}^T$, principal component regression (PCR)[11,16] coefficients are given by

$$\mathbf{B}^{PCR} = \mathbf{\Sigma_{VZ}}\mathbf{U}_{n_c}(\mathbf{D}_{n_c}^T\mathbf{D}_{n_c})^{-1}\mathbf{U}_{n_c}^T, \tag{3}$$

where only the diagonal matrix $\mathbf{D}_{n_c}^T\mathbf{D}_{n_c}$ has to be inverted. The projection to a subspace of maximum data variation can also be done for the data matrix $\mathbf{V}$. In this case, the dimensionality reduction using the new basis $\mathbf{P}_{n_c}$ is mainly intended to remove noise and minor consistency errors from the velocity fields, resulting in compact representations of the internal motion.[10,17] Now, rephrasing of (2) gives

$$\mathbf{B}^{PCA} = \mathbf{P}_{n_c}(\mathbf{P}_{n_c}^T\mathbf{\Sigma_{VZ}}\mathbf{\Sigma_{ZZ}}^{-1}). \tag{4}$$

Using the new basis $\mathbf{P}_{n_c}$ to project the motion data does not influence the rank of $\mathbf{\Sigma_{ZZ}}$, so we still have to account for the multi-collinearity problem mentioned above. Here, we again approximate $\mathbf{\Sigma_{ZZ}}$ by $\mathbf{\Sigma_{ZZ}} + \gamma\mathbf{I}$. As an alternative, it would also be possible to combine $\mathbf{B}^{PCA}$ and $\mathbf{B}^{PCR}$ to perform dimensionality reduction of both the velocity fields and the surrogate data.[14]

2.1.2 Regression based on Partial Least Squares (PLS)

A major problem of PCA-based regression approaches is that the PCA is usually performed on the input and/or output data separately. In contrast, partial least squares (PLS) searches for orthonormal bases $\mathbf{U}_{n_c} := (\mathbf{u}_1, \ldots, \mathbf{u}_{n_c})$ and $\mathbf{P}_{n_c} := (\mathbf{p}_1, \ldots, \mathbf{p}_{n_c})$ consisting of pairs $\mathbf{u}_i$ and $\mathbf{p}_i$ that maximize the cross-covariance $\rho_i = \mathbf{u}_i^T\mathbf{\Sigma_{ZV}}\mathbf{p}_i$. It can be shown[18] that the directions sought are solutions of the eigenvector problem

$$\begin{cases} \mathbf{\Sigma_{ZV}}\mathbf{\Sigma_{VZ}}\mathbf{u}_i &= \rho^2\mathbf{u}_i \\ \mathbf{\Sigma_{VZ}}\mathbf{\Sigma_{ZV}}\mathbf{p}_i &= \rho^2\mathbf{p}_i. \end{cases} \tag{5}$$

Finally, for defining the regression coefficients the new basis $\mathbf{U}_{n_c}$ is used:

$$\mathbf{B}^{PLS} = \mathbf{\Sigma_{VZ}}\mathbf{U}_{n_c}(\mathbf{U}_{n_c}^T\mathbf{\Sigma_{ZZ}}\mathbf{U}_{n_c})^{-1}\mathbf{U}_{n_c}^T. \tag{6}$$

For calculating equation the eigenvectors and eigenvalues of (5) we use the non-linear iterative partial least squares algorithm (NIPALS), which is able to handle large matrices $\mathbf{V}$ and $\mathbf{Z}$.[19]

2.1.3 Regression based on Canonical Correlation Analysis (CCA)

Another way of taking into account the structure of the velocity fields and the surrogate signal is to perform a canonical correlation analysis (CCA). CCA aims at finding directions $\mathbf{u}_i$ and $\mathbf{p}_i$ that maximize the correlation $\rho_i = \frac{\mathbf{u}_i^T\mathbf{\Sigma_{ZV}}\mathbf{p}_i}{\sqrt{\mathbf{u}_i^T\mathbf{\Sigma_{ZZ}}\mathbf{u}_i\mathbf{p}_i^T\mathbf{\Sigma_{VV}}\mathbf{p}_i}}$ of the projected data. $\mathbf{u}_i$ and $\mathbf{p}_i$ can be retrieved by solving the eigenvalue problem:[18]

$$\begin{cases} \mathbf{\Sigma_{ZZ}}^{-1}\mathbf{\Sigma_{ZV}}\mathbf{\Sigma_{VV}}^{-1}\mathbf{\Sigma_{VZ}}\mathbf{u}_i &= \rho^2\mathbf{u}_i \\ \mathbf{\Sigma_{VV}}^{-1}\mathbf{\Sigma_{VZ}}\mathbf{\Sigma_{ZZ}}^{-1}\mathbf{\Sigma_{ZV}}\mathbf{p}_i &= \rho^2\mathbf{p}_i. \end{cases} \tag{7}$$

Here we encounter the same problem as in (2): The inverse of covariance matrix $\mathbf{\Sigma_{ZZ}}$ (and $\mathbf{\Sigma_{VV}}$) has to be calculated. We deal with this problem by reducing the dimensionality of $\mathbf{Z}$ (and $\mathbf{V}$) by performing a PCA first.[13] Having determined a new basis $\mathbf{U}_{n_c}$, matrix $\mathbf{B}^{CCA}$ is defined in the same way as $\mathbf{B}^{PLS}$ in (6):

$$\mathbf{B}^{CCA} = \mathbf{\Sigma_{VZ}}\mathbf{U}_{n_c}(\mathbf{U}_{n_c}^T\mathbf{\Sigma_{ZZ}}\mathbf{U}_{n_c})^{-1}\mathbf{U}_{n_c}^T. \tag{8}$$

Table 1. Landmark-based target registration errors, obtained for the surrogate-based estimation of inner lung motion as part of the leave-out tests, listed for the different regression approaches and the two high-dimensional surrogates (sampled skin surface: 100 points, All points), given as mean±standard deviation for the ten patients considered.

	Landmark-based Target-Registration-Error [mm]		
Motion Estimation	**EI → EE** 100 points/All points	**EI → MI** 100 points/All points	**EI → ME** 100 points/All points
No motion estimation	6.80 ± 1.80	4.88 ± 1.20	2.50 ± 0.60
Intra-patient registration	1.37 ± 0.16	1.57 ± 0.14	1.50 ± 0.17
Diffeomorphic estimation framework; regression coefficients = ...			
$\mathbf{B}^{OLS}$	$1.89 \pm 0.32/-$	$1.85 \pm 0.34/-$	$1.82 \pm 0.20/-$
$\mathbf{B}^{PCA}$	$1.79 \pm 0.32/-$	$1.80 \pm 0.32/-$	$1.75 \pm 0.21/-$
$\mathbf{B}^{PCR}$	$1.79 \pm 0.23/1.79 \pm 0.23$	$1.80 \pm 0.29/1.83 \pm 0.23$	$1.70 \pm 0.21/1.67 \pm 0.19$
$\mathbf{B}^{PLS}$	$1.79 \pm 0.23/1.74 \pm 0.22$	$1.79 \pm 0.29/1.77 \pm 0.25$	$1.61 \pm 0.14/1.65 \pm 0.16$
$\mathbf{B}^{CCA}$	$1.82 \pm 0.35/1.71 \pm 0.25$	$1.82 \pm 0.32/1.79 \pm 0.21$	$1.71 \pm 0.23/1.67 \pm 0.21$

2.2 Experiments

An evaluation of the different regression approaches was carried out on 4D CT data sets of 10 lung tumor patients (10-14 states, avg. spatial resolution 512×512×272 voxel and spacing 1×1×1.5 mm). Due to the lack of real data for the patients considered, a simulated multi-dimensional surrogate signal had to be used. For this purpose, a range image-based tracking of the raising/lifting of the chest wall was implemented using the patient's 4D CT data sets. Assuming a range imaging sensor positioned above the patient's chest, rays originating from n_{sur} points across the sensor plane are traced in anterior-posterior direction until they intersect with the chest wall. The air-to-soft tissue intersection is detected with subvoxel accuracy by using linear interpolation and a heuristically chosen threshold of −500 HU. Two different spatial samplings of the chest wall area were simulated: (1) $n_{sur} = 100$ equally spread points across a rectangular, patient-specific region of interest (ROI), and (2) all ROI points ($n_{sur} = 38000$ on average).

Using the state at end-inspiration (EI) as a reference, leave-out tests for all regression approaches and patients were performed to assess the surrogate-based motion estimation accuracy between EI and the left-out states of end-expiration (EE), mid-inspiration (MI), and mid-expiration (ME). Estimation of the motion between EI and EE is used to evaluate the extrapolation performance based on surrogate measurements not included in the training signal interval, whereas the other two cases are useful for analyzing the interpolation capabilities. The estimation accuracy was evaluated by computing a target registration error using manually defined landmark correspondences (70 landmarks per patient and breathing state). For this work, the number of components n_c used for each patient/experiment was optimized with respect to this registration error. A suitable weighting parameter γ for the Tikhonov regularization was chosen heuristically based on the condition number of the matrix to be inverted.

3. RESULTS

The results of the leave-out experiments are summarized in Table 1 and Figure 1. Results for $\mathbf{B}^{OLS}$ and $\mathbf{B}^{PCA}$ are only available for the 100 point skin surface sampling due to the high computational costs of calculating $\mathbf{\Sigma_{ZZ}}^{-1}$ in (2) and (4). On the one hand, Table 1 shows that using subspace methods leads to improved mean estimation accuracy compared to results obtained by standard OLS regression ($\mathbf{B}^{OLS}$). However, only the accuracy improvements for $\mathbf{B}^{PCA}$ are statistically significant (paired t-test, $p < 0.05$) for all three experiments (EE: $p = 0.006$, MI: $p = 0.001$, ME: $p = 0.002$). The differences between the various subspace methods are not significant (see Figure 1(a)), which suggests that using more elaborated methods like PLS and CCA instead of PCA/PCR might not be necessary in general. Our results also suggest that (on average) increasing the number of sampling points does not significantly improve the estimation accuracy (e.g. $\mathbf{B}^{CCA}$/EE: 1.82 ± 0.35 vs. 1.71 ± 0.25, $p = 0.26$). But there are differences between the patients included in our study. As an example,

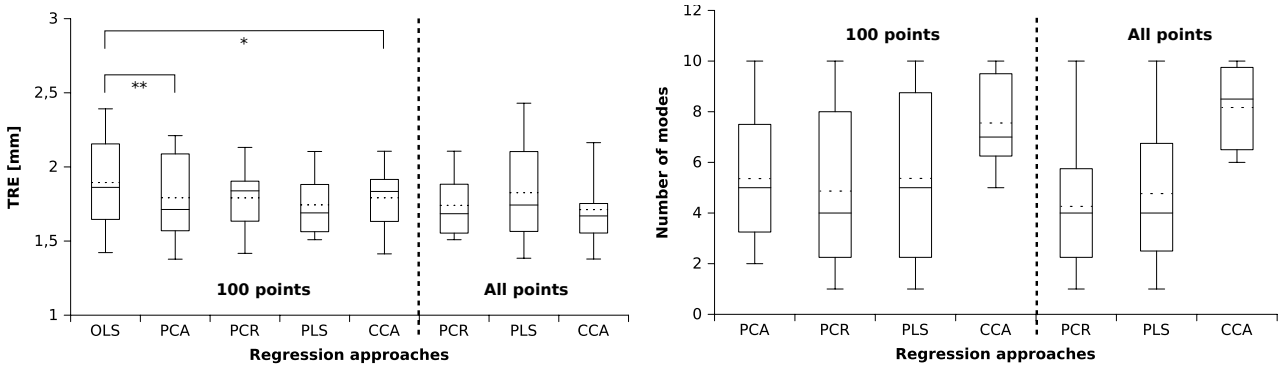

(a) (b)

Figure 1. Results of the surrogate-based estimation of lung motion fields between EI and EE for all patients. The dashed lines denote the mean values from Table 1 and 2. (a) Visualization of the landmark-based target registration errors (TRE) for the different regression approaches and the two high-dimensional surrogates (sampled skin surface: 100 points, All points). The asterisks indicate statistically significant differences (paired t-test, $p < 0.05$). *: $p = 0.046$, **: $p = 0.006$. (b) Optimized number of modes used for each subspace regression approach to obtain the lung motion fields between EI and EE.

Table 2. Number of modes used for each subspace regression approach to obtain the results reported in Table 1. Number of modes were optimized with respect to the TRE and the results are given as mean±standard deviation for the ten patients considered.

	Number of modes used		
Subspace approach	**EI → EE** 100 points/All points	**EI → MI** 100 points/All points	**EI → ME** 100 points/All points
$\mathbf{B}^{PCA}$	$5.40 \pm 2.84/-$	$4.90 \pm 3.32/-$	$4.20 \pm 3.46/-$
$\mathbf{B}^{PCR}$	$4.90 \pm 3.57/4.30 \pm 2.63$	$7.50 \pm 3.98/8.50 \pm 3.89$	$7.50 \pm 3.98/5.00 \pm 2.49$
$\mathbf{B}^{PLS}$	$5.40 \pm 3.63/4.80 \pm 2.90$	$5.30 \pm 3.47/5.60 \pm 1.84$	$4.80 \pm 3.36/4.40 \pm 2.84$
$\mathbf{B}^{CCA}$	$7.60 \pm 1.84/8.20 \pm 1.69$	$8.60 \pm 2.84/8.90 \pm 2.34$	$8.50 \pm 1.84/9.30 \pm 2.16$

for patient 01 (Figure 2) using only 100 chest points leads to a visible underestimation of the motion amplitude for the surrogate-based results compared to the displacement field estimated with our intra-patient registration algorithm. In this case, increasing the number of sampling points clearly reduces the underestimation. In contrast, for the motion fields of patient 05 shown in Figure 3, no major differences between the use of different approaches and surface samplings are observable. As the results in Table 2 and Figure 1 (b) show, the optimal number of components used differs for different patients, approaches, and/or test cases. For example, on average five components were used for calculating $\mathbf{B}^{PCR}$ (EI → EE case with 100 surface points), with a maximum of 10 components and a minimum of 1 component.

4. CONCLUSIONS

External breathing signals (surrogates of internal motion patterns) are utilized to guide modern RT techniques. Following the trend toward multi-dimensional surrogates, we extended our diffeomorphic standard MLR-based estimation framework by incorporating state-of-the-art subspace-based regression methods, which aim at exploiting the hidden structure of the training data to improve the use of information provided by high-dimensional surrogate and internal motion representations.

Our results show that, in general, subspace-based approaches have the potential to significantly improve the estimation accuracy when compared to standard OLS regression. However, based on our results, it is hard to choose one subspace approach with a certain configuration (number of components, surface sampling, ...)

that would work equally well for all patients. Therefore, future work will include a further investigation of the number of components needed for each approach. The goal should be to define automatic selection criteria like percentage of explained variability for PCA-based approaches, because an optimization with respect to the TRE using manually determined landmarks, as done for this study, is not feasible in clinical practice. We also plan to extend our evaluation to include an investigation of the motion estimation accuracy in the presence of intra- and inter-cycle motion variability and the use of real range imaging data instead of image-based simulations. Furthermore, we only have discussed the primal forms of the different regression approaches so far, but all of them can be expressed solely in terms of inner products resulting in a dual version.[20] Then, the well-known kernel trick can be utilized to perform non-linear regression.[21]

ACKNOWLEDGMENTS

This work is supported by the German Research Foundation DFG (HA 2355/9-2).

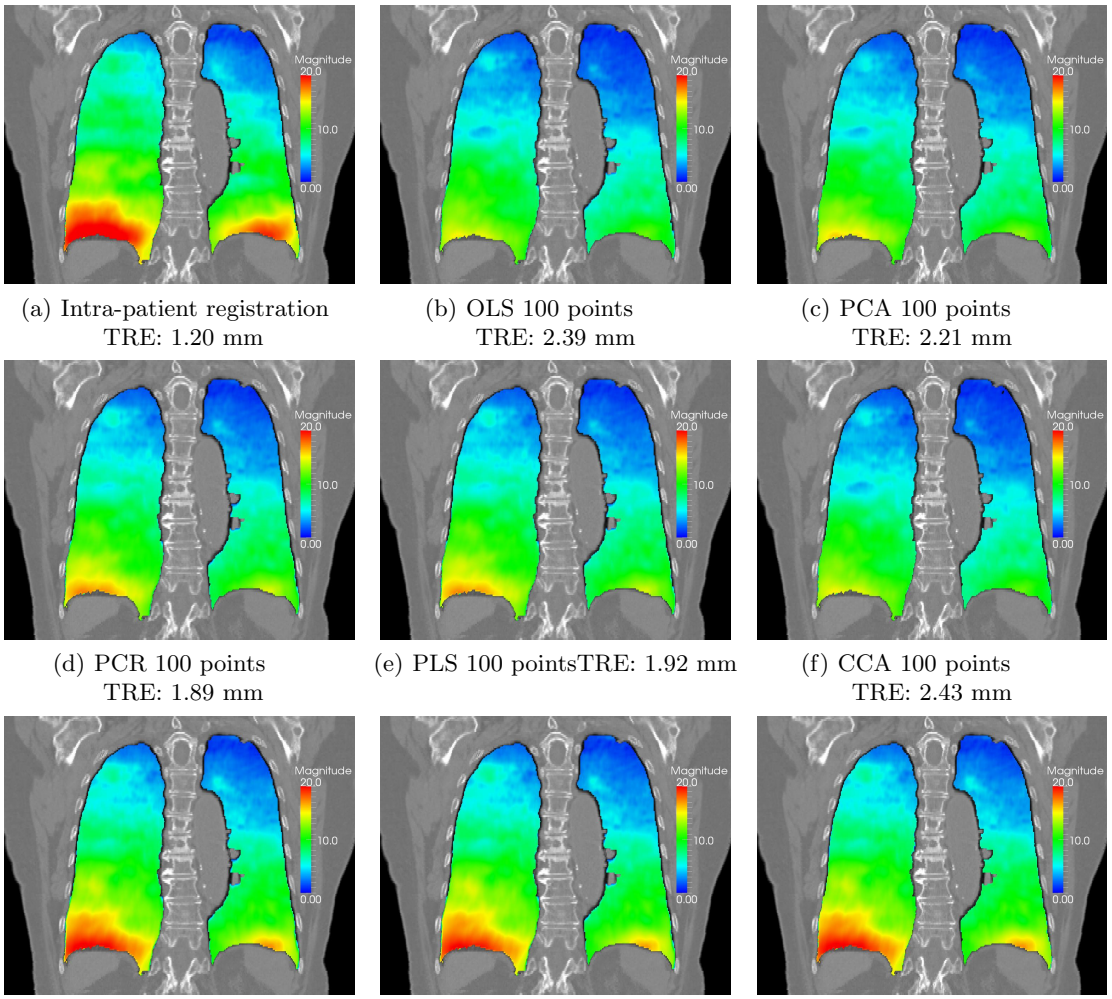

(a) Intra-patient registration TRE: 1.20 mm
(b) OLS 100 points TRE: 2.39 mm
(c) PCA 100 points TRE: 2.21 mm
(d) PCR 100 points TRE: 1.89 mm
(e) PLS 100 pointsTRE: 1.92 mm
(f) CCA 100 points TRE: 2.43 mm
(g) PCR 42000 points TRE: 1.53 mm
(h) PLS 42000 points TRE: 1.52 mm
(i) CCA 42000 points TRE: 1.53 mm

Figure 2. Visualization of the lung motion between EI and EE of patient 01 estimated with intra-patient registration (a) and the different regression approaches/surface samplings (b)–(i).

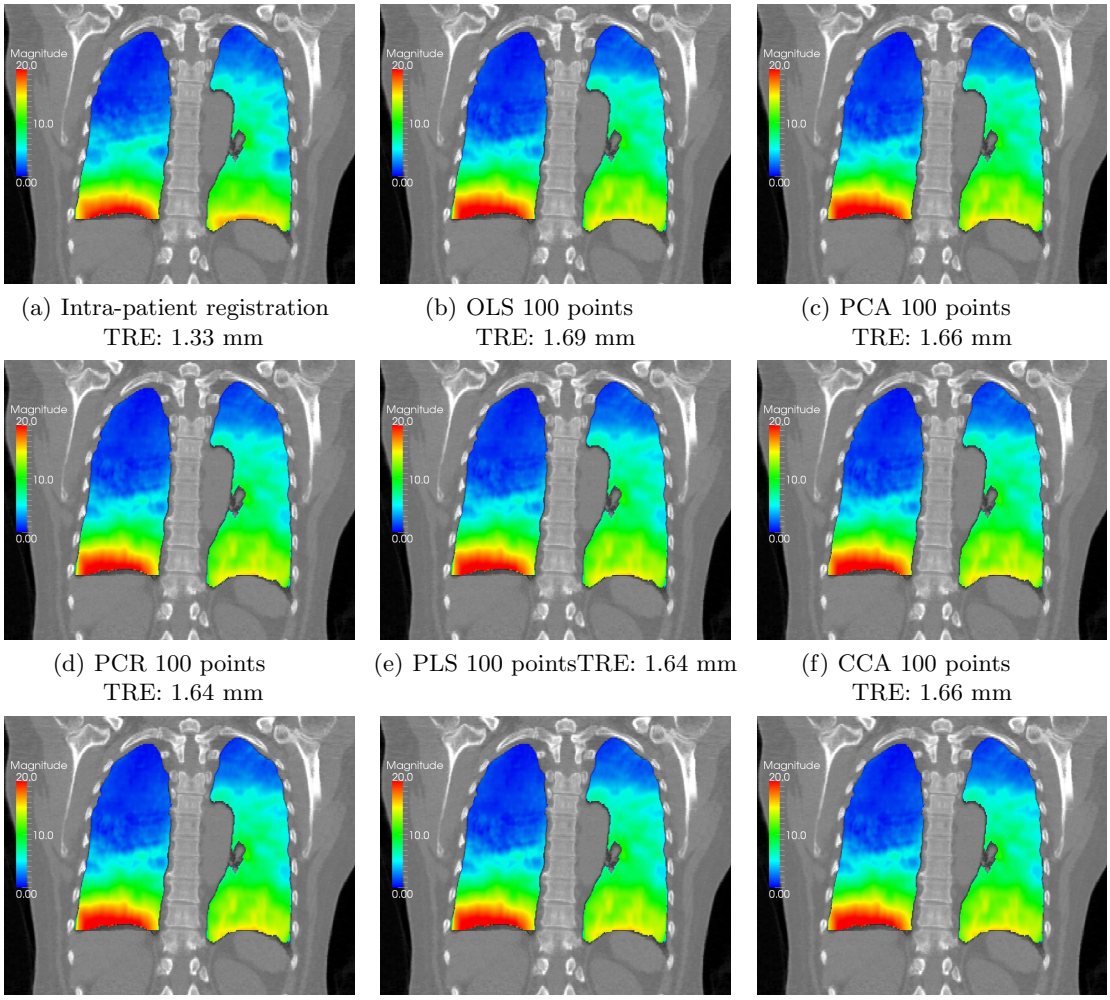

(a) Intra-patient registration TRE: 1.33 mm

(b) OLS 100 points TRE: 1.69 mm

(c) PCA 100 points TRE: 1.66 mm

(d) PCR 100 points TRE: 1.64 mm

(e) PLS 100 pointsTRE: 1.64 mm

(f) CCA 100 points TRE: 1.66 mm

(g) PCR 32200 points TRE: 1.65 mm

(h) PLS 32200 points TRE: 1.64 mm

(i) CCA 32200 points TRE: 1.62 mm

Figure 3. Visualization of the lung motion between EI and EE of patient 05 estimated with intra-patient registration (a) and the different regression approaches/surface samplings (b)–(i).

REFERENCES

[1] Keall, P. J., Mageras, G., Balter, J. M., et al., "The management of respiratory motion in radiation oncology report of AAPM task group 76," *Medical Physics* **33**(10), 3874–3900 (2006).

[2] Li, G., Citrin, D., Camphausen, K., et al., "Advances in 4D medical imaging and 4D radiation therapy.," *Technology in Cancer Research and Treatment* **7**(1), 67–81 (2008).

[3] McClelland, J., Hawkes, D., Schaeffter, T., and King, A., "Respiratory motion models: A review," *Medical Image Analysis* **17**(1), 19 – 42 (2013).

[4] Schaller, C., Penne, J., and Hornegger, J., "Time-of-flight sensor for respiratory motion gating.," *Medical Physics* **35**(7), 3090–3093 (2008).

[5] Werner, R., Wilms, M., Ehrhardt, J., Schmidt-Richberg, A., Blendowski, M., and Handels, H., "A Diffeomorphic MLR Framework for Surrogate-based Motion Estimation and Situation-adapted Dose Accumulation," in [*Image-Guidance and Multimodal Dose Planning in Radiation Therapy: a MICCAI Workshop - MICCAI 2012*], 42–49 (2012).

[6] Schmidt-Richberg, A., Ehrhardt, J., Werner, R., and Handels, H., "Diffeomorphic diffusion registration of lung CT images," in [*Workshop Medical Image Analysis for the Clinic: A Grand Challenge - MICCAI 2010*], 55–62 (2010).

[7] Beg, M. F., Miller, M. I., Trouvé, A., and Younes, L., "Computing large deformation metric mappings via geodesic flows of diffeomorphisms," *International Journal of Computer Vision* **61**(2), 139–157 (2005).

[8] Arsigny, V., Commowick, O., Pennec, X., and Ayache, N., "A log-Euclidean framework for statistics on diffeomorphisms," in [*MICCAI 2006*], *LNCS* **4190**, 924–931, Springer (2006).
[9] King, A., Buerger, C., Tsoumpas, C., Marsden, P., and Schaeffter, T., "Thoracic respiratory motion estimation from MRI using a statistical model and a 2-D image navigator," *Medical Image Analysis* **16**(1), 252 – 264 (2012).
[10] Zhang, Q., Hu, Y.-C., Liu, F., Goodman, K., Rosenzweig, K., and Mageras, G., "Correction of motion artifacts in cone-beam CT using a patient-specific respiratory motion model.," *Medical Physics* **37**(6), 2901–2909 (2010).
[11] Klinder, T., Lorenz, C., and Ostermann, J., "Prediction framework for statistical respiratory motion modeling.," in [*MICCAI 2010*], *LNCS* **6363**, 327–334 (2010).
[12] Malinowski, K. T., McAvoy, T. J., George, R., Dieterich, S., and D'Souza, W. D., "Mitigating errors in external respiratory surrogate-based models of tumor position," *International Journal of Radiation Oncology*Biology*Physics* **82**(5), 709–716 (2012).
[13] Gao, G., McClelland, J., Tarte, S., Blackall, J., and Hawkes, D., "Modelling the respiratory motion of the internal organs by using Canonical Correlation Analysis and dynamic MRI," in [*The First International Workshop on Pulmonary Image Analysis, MICCAI 2008*], 145–154 (2008).
[14] Liu, X., Oguz, I., Pizer, S. M., and Mageras, G. S., "Shape-correlated deformation statistics for respiratory motion prediction in 4D lung," in [*SPIE Medical Imaging 2010: Visualization, Image-Guided Procedures, and Modeling*], *Proc. of SPIE* **7625** (2010).
[15] Hastie, T., Tibshirani, R., and Friedman, J., [*The Elements of Statistical Learning: Data Mining, Inference, and Prediction*], Springer, 2nd ed. (2009).
[16] Jolliffe, I., [*Principal Component Analysis*], Springer, 2nd ed. (2002).
[17] Li, R., Lewis, J. H., Jia, X., Zhao, T., Liu, W., Wuenschel, S., Lamb, J., Yang, D., Low, D. A., and Jiang, S. B., "On a PCA-based lung motion model," *Physics in Medicine and Biology* **56**(18), 6009 (2011).
[18] Borga, M., Landelius, T., and Knutsson, H., "A Unified Approach to PCA, PLS, MLR and CCA," Tech. Rep. LiTH-ISY-R-1992, Linköping University, The Institute of Technology (1997).
[19] Rosipal, R. and Krämer, N., "Overview and recent advances in partial least squares," in [*Subspace, Latent Structure and Feature Selection*], *LNCS* **3940**, 34–51, Springer (2006).
[20] Bie, T. D., Cristianini, N., and Rosipal., R., "Eigenproblems in pattern recognition," in [*Handbook of Geometric Computing: Applications in Pattern Recognition, Computer Vision, Neuralcomputing, and Robotics*], 129–170, Springer (2005).
[21] He, T., Xue, Z., Xie, W., and Wong, S., "Online 4-D CT estimation for patient-specific respiratory motion based on real-time breathing signals," in [*MICCAI 2010*], *LNCS* **6363**, 392–399, Springer (2010).